OPEN ACCESS
Journal of Porphyrins and Phthalocyanines
*J. Porphyrins Phthalocyanines* 2025; **29**: A–O
DOI: 10.1142/S1088424625500130
(pp. 15)



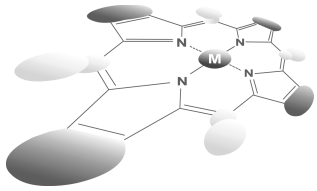


# Effect of porphyrin metalation and synergistic combination with fluconazole in antifungal PDT against *Candida spp*

**Margaret W. Murage[a,b], Edith K. Amuhaya*[,b], Betty N. Mbatia[b] and Edward K. Muge[a]**

[a]*University of Nairobi, P.O Box 30197-00100, Nairobi, Kenya*
[b]*United States International University-Africa, P. O. Box 14634-00800, Nairobi, Kenya*

*Received 19 December 2024*
*Accepted 14 January 2025*

**ABSTRACT:** Candidiasis, a common fungal infection, presents significant treatment challenges due to the increasing resistance of *Candida* species to conventional antifungal medications. Photodynamic antimicrobial chemotherapy (PACT) offers a promising alternative by utilizing photosensitizers activated by specific wavelengths of light to generate reactive oxygen species (ROS), which effectively eradicate pathogens. This study investigated the efficacy of PACT using porphyrin-based photosensitizers, including free base and metallated porphyrins (zinc, indium, and gallium derivatives), both alone and in combination with fluconazole, against two *Candida* strains: *Candida albicans* ATCC 10231 and *Candida krusei* ATCC 6258. The photosensitizers were activated using a 430 nm LED, delivering a fluence of 180 J/cm$^2$. Post-treatment, the antimicrobial effect was assessed by quantifying colony-forming units (CFU). **P-InCl** exhibited potent antifungal activity, achieving a 5-log reduction in colony-forming units (CFU) for *Candida albicans* (*C. albicans*) and a 4.5-log reduction for *Candida krusei* (*C. krusei*) following PACT alone. When combined with fluconazole, **P-InCl** demonstrated enhanced efficacy, achieving complete eradication of *C. albicans* within 15 minutes and a 5-log reduction for the fluconazole-resistant *C. krusei* within 30 minutes. These findings highlight the potential of PACT, particularly when combined with antifungal agents, as an effective strategy for treating resistant or persistent *Candida* infections, suggesting a path toward clinical implementation in antifungal therapies.

**KEYWORDS:** antifungal resistance, Candida albicans, Candida krusei, fluconazole, photodynamic antimicrobial chemotherapy, porphyrins



## INTRODUCTION

*Candida* species (*spp*) are typically harmless fungi that reside on human skin and mucosal surfaces [1]. However, under certain conditions such as prolonged antibiotic therapy or in immuno-compromised individuals, these fungi can become pathogenic, causing infections and spreading to other parts of the body. This shift can lead to infections that vary from mild skin and mucosal lesions to severe systemic invasions [2]. *Candida albicans* (*C. albicans*) are part of the human microbiota, typically found in the mucosa of the oral cavity and the female urogenital tract [3]. While *C. albicans* is the most frequent cause of candidiasis, a significant number of infections have been attributed to non-albicans Candida (NAC) species, particularly *Candida krusei* (*C. krusei*) which is recognized for its significant resistance to current antifungal drugs such as fluconazole [4]. Infections caused by *C. krusei* are associated with a high mortality rate, ranging from 40 to 58% [5]. This fungus can exist transiently in various sites within the human microbiota, but it is most commonly isolated from the oral mucosa

*Correspondence to: Edith K. Amuhaya, e-mail: eamuhaya@usiu.ac.ke

[6]. The candidiasis caused by *C. krusei* is particularly concerning due to the severity of the infections and the challenges in treatment [7]. Both *C. albicans* and *C. krusei* have been extensively studied for their ability to cause severe infections and develop biofilms on both biotic and abiotic surfaces, which significantly contribute to antifungal resistance [6, 8, 9]. These biofilms create a protective matrix that restricts drug penetration, supports reduced metabolic activity, and enhances the expression of drug-efflux pumps and stress-response genes, making infections difficult to treat and prone to recurrence [9, 10].

Common antimycotic drugs for controlling Candida infections can be classified as polyenes, nucleoside analogues, echinocandins, allylamines, and azoles [11]. Azoles are further classified as imidazoles (clotrimazole, miconazole and ketoconazole) and triazoles (itraconazole and fluconazole). Approved by the FDA in 1990, Fluconazole, commonly known as Diflucan®, is an antifungal medication used to treat both systemic and superficial fungal infections across various tissues, including the skin (dermatophytosis), mucosal membranes (oral thrush and vaginal candidiasis), and deeper tissues or organs such as the central nervous system (cryptococcal meningitis) and blood (systemic candidiasis) [12]. One of the key advantages of fluconazole is its ability to be administered orally, making it more convenient compared to other antifungal treatments [12].

Although antifungals like fluconazole are effective, they are associated with several drawbacks. First, fungi and their human hosts are both eukaryotes and this limits the number of drugs that can exhibit selective toxicity [13]. Secondly, some antifungals that share toxicity with human cells must be administered at low doses, resulting in extended treatment durations of up to 12 months [14]. This prolonged treatment period often leads to patient non-compliance, resulting in treatment abandonment, high recurrence rates, and the potential for exacerbating resistance to antifungal agents, as incomplete treatment courses may allow resistant fungal strains to proliferate. Long-term use of antifungals is particularly problematic for certain patients, for example, the elderly who may experience drug interactions with other medications, and for patients with abnormal liver function [15]. Lastly, when it comes to eliminating formed biofilms, pharmacological approaches such as the use of antifungal agents like fluconazole or amphotericin B are often unsuccessful [16]. This is primarily due to the inherent resistance of biofilms, which is attributed to several factors, including their dense extracellular matrix that limits drug penetration, and altered microenvironment within the biofilm, making them less susceptible to antifungal agents. The ideal antifungal therapy should be fungicidal, meaning it can effectively kill the fungus, have a short duration, be easy to administer, cause minimal adverse side effects, and be affordable [14]. Consequently, novel antifungal strategies are required to control the spread of fungal infections.

One promising approach is photodynamic antimicrobial chemotherapy (PACT), which involves the use of a photosensitizer (PS), light of a specific wavelength, and molecular oxygen [17]. When the PS absorbs light, it transitions from its ground state to an excited singlet state. It can then return to the ground state via two mechanisms that produce reactive oxygen species (ROS) [18]. In the type I mechanism, charge transfer to a substrate generates superoxide radicals ($O_2$–•), hydrogen peroxide ($H_2O_2$), and hydroxyl radicals (HO•). In the type II mechanism, energy transfer directly to molecular oxygen ($3O_2$) produces singlet oxygen ($^1O_2$) [19]. These ROS have potent antimicrobial effects, disrupting cellular structures and functions. Notably, numerous PACT studies have demonstrated that *Candida* species, including those that form biofilms, can be effectively photoinactivated both *in vitro* and *in vivo* [20, 21]. Biofilms are a major challenge in *Candida* treatment due to their protective matrix, which restricts antifungal penetration thereby promoting resistance [22]. PACT has shown the potential to overcome this challenge by generating ROS that penetrate biofilms and disrupt their structural integrity, thereby enhancing drug delivery and efficacy [23]. This unique ability to target both planktonic cells and biofilm-encased cells positions PACT as a promising strategy to address the persistent challenge of biofilm-associated *Candida* infections [24].

Porphyrins are compounds reported to be useful in many biomedical applications, such as their use as photosensitizers in PACT, due to their unique and highly desirable properties in cells [25, 26]. One of the primary advantages of porphyrins is their low toxicity to living cells, making them safe for medical use [26, 27]. Research has also shown that porphyrins possess broad-spectrum antimicrobial activity, effectively targeting a wide range of microorganisms, including *C. albicans* and *C. krusei* [28. 29, 30]. In this study, we investigated the effects of PACT using a free base porphyrin and its Zn, indium, and gallium metallated analogues (Scheme 1). (5,10,15,20-tetra(4-bromophenyl) porphyrin **(P-2H)**, Zn 5,10,15,20-tetra(4-bromophenyl) porphyrin **(P-Zn)**, indium (III) chloride 5,10,15,20-tetra(4-bromophenyl) porphyrin **(P-InCl)**, and gallium(III) chloride 5,10,15,20-tetra(4-bromophenyl) porphyrin **(P-GaCl)**, alone and in combination with the antifungal agent fluconazole, against *C. albicans* and *C. krusei* were evaluated. Bromine-substituted porphyrins and their metallated derivatives were selected because the bromine atoms at the *meso*-positions introduce a heavy atom effect that promotes intersystem crossing (ISC), which enhances the production of reactive oxygen species (ROS) upon light activation [30, 31]. This is crucial in PACT applications as it leads to higher singlet oxygen yields, an important factor for the effective photodynamic inactivation of microorganisms [34]. The incorporation of metals further enhances singlet oxygen yield and enhances cellular uptake, intensifying the cytotoxic effects on *Candida*

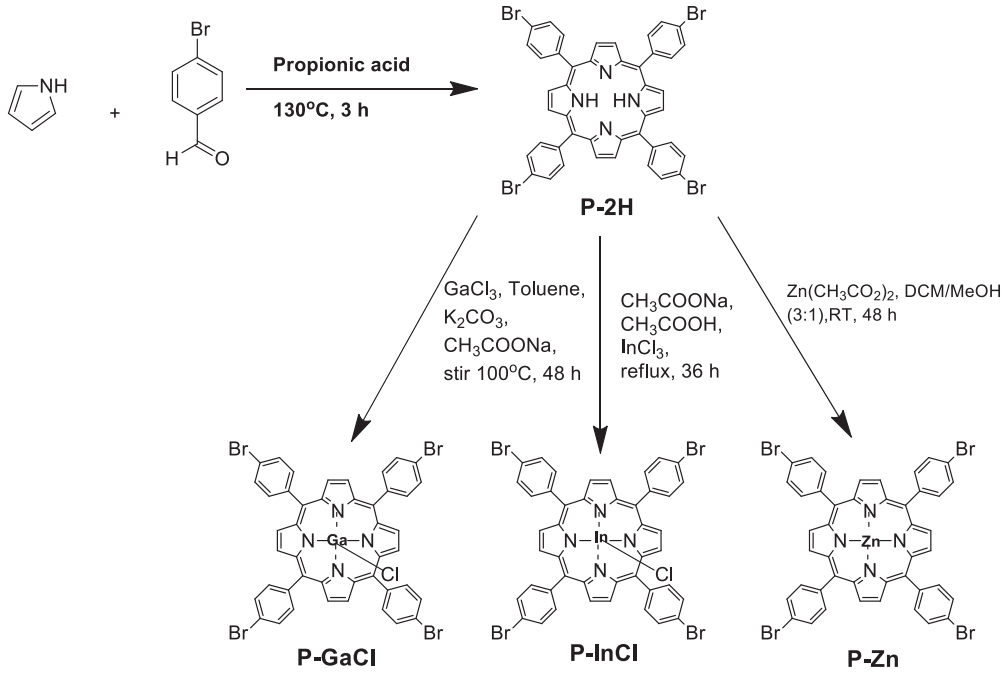


**Scheme 1.** Synthetic pathway of **P-2H**, **P-Zn**, **P-InCl**, and **P-GaCl**.

cells [35]. While some of these porphyrins have been studied in other applications, such as PDT, their antifungal effects, particularly against *Candida* species, remain largely unexplored [30, 32]. Recent research has also reported the combination of PACT with antifungal agents to enhance fungal inactivation and prevent regrowth once the photoinactivation process is complete [30]. By implementing this combined approach, it is possible to reduce the reliance on antifungals and consequently address the issue of multidrug resistance.

## MATERIAL AND METHODS

### Chemicals and reagents

All chemicals and reagents used in this study were of high purity, and the organic solvents were of analytical grade. The chemicals included pyrrole from Merck (USA), 4-bromobenzaldehyde, zinc(II) acetate (ZnOAc), indium(III) chloride ($InCl_3$), gallium (III) chloride ($GaCl_3$), sodium hydroxide (NaOH), anhydrous sodium sulfate ($NaSO_4$), dimethyl sulfoxide (DMSO), and hydrated sodium acetate ($NaOAc•3H_2O$), all sourced from Sigma-Aldrich (USA). Acids and solvents including propionic acid, glacial acetic acid, dichloromethane, methanol, ethyl acetate, and ethanol were procured from Loba Chemie (India) and Sigma Aldrich (USA). Silica gel 60 for column chromatography was purchased from Thermo Fisher Scientific (USA). Phosphate-buffered saline (PBS) and Yeast Peptone Dextrose (YPD) broth, Yeast Peptone Dextrose (YPD) agar, Sabouraud Dextrose Broth (SDB), and Sabouraud Dextrose Agar (SDA), were supplied by HiMedia Laboratories (India). Fluconazole was acquired from Scientific Laboratory Supplies (UK).

### Instrumentation

UV-Vis absorption spectra were recorded using a Shimadzu UV-1800 spectrophotometer (Shimadzu, Japan) with a 1 cm path length cuvette. Fluorescence excitation and emission spectra were obtained from a Shimadzu RF-6000 spectro-fluorophotometer (Shimadzu, Japan). Singlet oxygen generation in DMF was quantified using an ultrasensitive Germanium detector (Edinburgh Instruments, UK) equipped with a 1000 nm long-pass filter (Omega, USA) and a 1270 nm band pass filter (Omega, USA). Mass spectrometry analysis was performed using a Bruker AutoFLEX III Smartbeam MALDI-TOF instrument (Bruker Corporation, Massachusetts, USA) with dithranol as the matrix in positive ion mode. Elemental analyses were conducted with a Vario EL III Microcube CHNS Analyzer (GmbH, Germany). Proton NMR spectra were recorded on a Bruker AVANCE II 80 MHz NMR spectrometer (Bruker Corporation, USA), using tetramethylsilane as the internal standard. Chemical bond identification and molecular structure analysis were carried out using a Jasco FT/IR-4700 FTIR spectrometer (Jasco Corporation, Japan). Fungal cell photo-irradiation was conducted with a 430 nm mounted LED (Thorlabs, USA) controlled by a T-cube LED driver (Thorlabs, USA). Optimal conditions for fungal cultures were maintained using a shaking incubator (Thermo Fisher Scientific, USA). Fungal growth was monitored by measuring

the optical density at 600 nm with a microplate reader (PerkinElmer, Inc., USA).

## Synthesis and characterization of photosensitizers

### *Synthesis of 5,10,15,20-tetra(4-bromophenyl) porphyrin (P-2H)*

4-bromobenzaldehyde (1.2 g, 30 mmol) was added to propionic acid (50 mL) and the reaction mixture was heated to 130 °C. To this mixture, freshly distilled pyrrole (0.4 ml, 30 mmol) was added gradually and the resulting mixture was stirred and refluxed for 3 h. The reaction was continuously monitored using TLC and UV-visible absorption spectroscopy. After the reaction was complete, the mixture was allowed to cool to room temperature before 50 mL of methanol was added to quench the reaction. The purple solid product was collected using vacuum filtration, washed with methanol, and dried in the open air. To further purify the product, it was subjected to elution in a column packed with silica gel using ethyl acetate: hexane (1:5 v/v) mobile phase to obtain the target product as a purple solid (**P-2H**).

Yield: 13% (0.72 g), UV/Vis ($CH_2Cl_2$) $\lambda_{max}$ nm ($\log_\varepsilon \times 10^4$): 418.5 (48.8), 515 (2.92), 549.5 (1.82), 590.5 (1.50), 646.5 (1.34). $^1$H NMR (80 MHz, $CD_2Cl_2$) δ 8.87 (s, 8H, β-Pyrrole), 8.10 (d, $J$ = 8.5 Hz, 8H, *ortho*-bromophenyl), 7.99-7.83 (m, 8H, meta-bromophenyl), -2.93 (s, 2H,-NH). MALDI- TOF-MS m/z: calcd = 930.34, found = 931.374 [M+H]. Calc. for $C_{44}H_{26}Br_4N_4$: C (56.81), H (2.82), N (6.02); found C (56.64), H (2.81), N (5.99). FTIR: 2928.38 $cm^{-1}$ (C–H stretching vibrations) from the aromatic groups, 1575.56 $cm^{-1}$ (C–H bending vibrations) within the aromatic system, 1344.14 $cm^{-1}$ (C–N stretching vibration) from the pyrrole ring, 1211.08 $cm^{-1}$ (aromatic C–Br stretching vibration), 842.74 $cm^{-1}$ (out-of-plane C–H bending vibrations) typical for substituted aromatic rings.

### *Synthesis of Zn 5,10,15,20-tetra(4-bromophenyl) porphyrin (P-Zn)*

**P-Zn** was synthesized by dissolving **P-2H** (0.2 g, 0.215 mmol) in a DCM/MeOH solvent mixture (3:1) and subsequent addition of zinc acetate (0.04 g, 0.8728 mmol). The resulting mixture was stirred at room temperature for 24 h. After completion, the reaction was quenched with water, dried over anhydrous $Na_2SO_4$ to remove traces of moisture, and the desired product was extracted using DCM. The crude product was purified using a silica gel column, with ethylacetate: hexane (1:7 v/v) mobile phase. The target porphyrin compound was obtained as a purple solid (**P-Zn**).

Yield: 84% (0.18 g), UV/Vis ($CH_2Cl_2$) $\lambda_{max}$ nm ($\log_\varepsilon$): 420 (48.4), 548 (2.54), 587 (1.18). $^1$H NMR (80 MHz, $CD_2Cl_2$) δ 8.94 (s, 8H, β-Pyrrole), 8.09 (d, $J$ = 8.4 Hz, 8H, ortho-bromophenyl), 7.89 (d, $J$ = 8.6 Hz, 8H, *meta*-bromophenyl). MALDI- TOF-MS, calc = 994.69, found = 994.349. Calc. for $C_{44}H_{24}Br_4ZnN_4$: C (53.18), H (2.43), N (5.64); found C (53.05), H (2.41), N (5.62). FTIR: 2919.70 $cm^{-1}$ (C–H stretching vibrations) from the aromatic groups, 1589.06 $cm^{-1}$ (C=C stretching vibrations) within the aromatic rings of the porphyrin macrocycle, 1469.49 $cm^{-1}$ (C–H bending vibrations) within the aromatic system, 1381.75 $cm^{-1}$ (C–N stretching vibration) from the pyrrole ring, 1252.54 $cm^{-1}$ (C–Br stretching vibration), 1059.69 $cm^{-1}$ (aromatic C–Br stretching vibration characteristic of bromophenyl groups), and 787.78 $cm^{-1}$ (out-of-plane C–H bending vibrations) typical for substituted aromatic rings.

### *Synthesis of indium(III) chloride 5,10,15,20-tetra (4-bromophenyl) porphyrin (P-InCl)*

**P-InCl** was synthesized following the procedure described by [36]. Specifically, 0.15 g (0.107 mmol) of **P-2H** was dissolved in 50 mL of acetic acid. This was followed by the addition of 0.219 g (1.612 mmol) of sodium acetate and 0.0594 g (0.268 mmol) of indium(III) chloride. The resulting mixture was refluxed for 36 h. The contents were then cooled to room temperature, mixed with water, dried over anhydrous $Na_2SO_4$ to remove traces of moisture, and extracted with DCM. The crude product was purified by passing it through a silica gel column using ethyl acetate: hexane (1:9 v/v) as the eluent, resulting in a purple solid (**P-InCl**).

Yield: 82% (0.09 g), UV/Vis ($CD_2Cl_2$) $\lambda_{max}$ nm ($\log_\varepsilon \times 10^4$): 430.5 (19.3), 561.5 (1.13), 609 (0.414). $^1$H NMR (80 MHz, $CD_2Cl_2$) δ 9.13 (s, 8H, β-Pyrrole) δ 8.26 (d, $J$ = 8.4 Hz, 4H, ortho-bromophenyl) δ 8.07-7.82 (m, 12H, meta and ortho-bromophenyl). MALDI- TOF-MS, calc = 1078.59, found = 1078.30. Calc. for $C_{44}H_{24}Br_4ClInN_4$: C (49.00), H (2.24), N (5.19). Found C (48.86), H (2.22), N (5.17). FTIR: 2917.77 $cm^{-1}$ (C–H stretching vibrations) from the aromatic groups, 1635.34 $cm^{-1}$ (C=C stretching vibrations) within the aromatic rings of the porphyrin macrocycle, 1462.74 $cm^{-1}$ (C–H bending vibrations) within the aromatic system, 1257.36 $cm^{-1}$ (C–Br stretching vibration), 1065.48 $cm^{-1}$ (C–O–C asymmetric stretching), and 797.42 $cm^{-1}$ (out-of-plane C–H bending vibrations) typical for substituted aromatic rings.

### *Synthesis of gallium(III) 5,10,15,20-tetra (4-bromophenyl) porphyrin (P-GaCl)*

**P-GaCl** was synthesized through the metalation reaction of **P-2H**. To synthesize this compound, **P-2H** (0.1 g, 0.12 mmol) was dissolved in 30 mL of toluene. $GaCl_3$ (0.59 g, 0.10 mmol), anhydrous $K_2CO_3$ (0.92 g, 2.2 mmol), and sodium acetate (0.17 g, 0.92 mmol) were added. The reaction mixture was then refluxed for 48 h under nitrogen. After cooling to room temperature, the

flask contents were neutralized with acetic and subjected to solvent extraction using toluene as the organic solvent. The organic layer was separated, washed with water to remove any residual impurities, and then dried over anhydrous $Na_2SO_4$ to remove traces of moisture. The dried extract was subjected to purification via column chromatography using methanol: dichloromethane (2:8 v/v) mobile phase. The resulting purified product was a purple solid (**P-GaCl**).

Yield: 82% (0.082 g), UV/Vis (CH2Cl2) $\lambda_{max}$ nm ($\log_\varepsilon \times 104$): 420.5 (22.8), 551 (1.82), 616 (1.04). $^1$H NMR (80 MHz, $CD_2Cl_2$) δ 9.11 (s, 8H, β-Pyrrole), 8.09 (d, $J$=8.1 Hz, 8H), 7.91 (d, $J$=8.4 Hz, 8H). MALDI-TOF-MS m/z: calcd=1034.49, found=999.321 [M–Cl]$^{+\cdot}$ Calc. for $C_{44}H_{24}Br_4ClGaN_4$: C (51.14), H (2.34), N (5.42); found C (51.04), H (2.33), N (5.39). FTIR: 2921.63 cm$^{-1}$ (C–H stretching vibrations) from the aromatic groups, 1641.13 cm$^{-1}$ (C=C stretching vibrations) within the aromatic rings of the porphyrin macrocycle, 1476.24 cm$^{-1}$ (C–H bending vibrations) within the aromatic system, 1298.82 cm$^{-1}$ (C–Br stretching vibration), 1064.51 cm$^{-1}$ (C–O–C asymmetric stretching vibration), and 796.46 cm$^{-1}$ (out-of-plane C–H bending vibrations) typical for substituted aromatic rings.

## Photo-physical studies

### *UV-Vis spectroscopy*

Measurements were conducted in dichloromethane (DCM) at room temperature using 10 mm quartz cell cuvettes (Hellma Analytics, Germany). Before sample analysis, the spectrophotometer was calibrated using a DCM blank as the reference. The samples, prepared at a concentration of 1 μM, were scanned and the spectra were recorded for further analysis.

### *Fluorescence spectroscopy and Fluorescence quantum yield*

Fluorescence measurements were performed at room temperature using solutions of both the sample and the standard in N, N-Dimethylformamide (DMF). The absorbance of each solution was measured with a UV-Vis spectrophotometer in the 350-700 nm range, ensuring concentrations had absorbance values below 0.1 to minimize inner filter effects. Fluorescence emission spectra were recorded at an excitation wavelength of 400 nm using 10 mm quartz cell cuvettes. The areas under the emission spectra were calculated, and the fluorescence quantum yield (ϕF) was determined using the comparative method described by Fery-Forgues and Lavabre [37], as shown in Eq. (1).

$$\phi_F = \phi F^{Std} \frac{F A^{Std} n^2}{F^{Std} A \left(n^{Std}\right)^2}. \quad (1)$$

Where F and $F^{Std}$ represent the areas under the fluorescence emission curves of the porphyrin and standard, respectively, while A and $A^{Std}$ denote the optical absorbance of the sample and standard, respectively, at the excitation wavelength. Furthermore, n and $n^{Std}$ correspond to the refractive indices of the solvent used to dissolve the sample and the standard, respectively. $\phi F^{Std}$ represents the fluorescence quantum yield for the standard. For these metallated porphyrins, zinc tetraphenylporphyrin (ZnTPP) ($\phi_F$=0.033) was used as the standard reference [38].

### *Singlet oxygen quantum yields*

The singlet oxygen quantum yield (ϕΔ) represents how effectively a molecule converts absorbed energy into singlet oxygen ($^1O_2$) from ground-state molecular oxygen ($O_2$). The ϕΔ value is largely dependent on the molecule's ability to undergo intersystem crossing (ISC) to the triplet excited state [39]. ISC, which increases ϕΔ, is typically enhanced by the heavy atom effect, influenced by the substituents and metal ions present in the porphyrins. The singlet oxygen quantum yield for the compounds was calculated using Eq. (2), with ZnTPP (ϕΔ=0.53) serving as the reference and 1,3-Diphenylisobenzofuran (DBPF) as the singlet oxygen quencher in dimethylformamide (DMF).

$$\varphi\Delta = \varphi_F^{Std} x \frac{B.I^{Std}}{B^{Std} \cdot l}. \quad (2)$$

B and $B^{Std}$ represent the photobleaching rates of the singlet oxygen quencher in the presence of the porphyrin derivatives and the standard, respectively. I and $I^{Std}$ denote the rates of light absorption by the sample and the standard, respectively.

## PACT and combined therapy

### *Fungal strains and photosensitizers*

Two fungal strains *Candida* species, *C. albicans* ATCC 10231 and *C.krusei* ATCC 6258 were used in this study. The strains were individually cultured in Yeast Peptone Dextrose (YPD) broth at 37 °C for 24 h for the phototoxicity experiments. Stock solutions of the synthesized PSs (500 μM) were prepared by dissolving them in a 5% dimethyl sulfoxide (DMSO) solution in phosphate-buffered saline (PBS) and stored in the dark at −20 °C. Before each assay, the stock solution was vortexed for 30 min at room temperature. Stock solutions of fluconazole were prepared by dissolving the drug in DMSO to achieve final concentrations of 1 mg/mL and stored at -20 °C. Photodynamic inactivation was performed using a light-emitting diode (LED) (430 nm excitation wavelength) with an irradiance at 0.05 W/cm$^2$ and a light dosage of 180 J/cm$^2$ for 60 min.

### *The minimum inhibitory concentrations (MIC) of fluconazole*

These were determined using the microdilution method [40]. *C. albicans* and *C. krusei* were individually grown on SDB for 24 h at 37 °C. The fungal cultures were then diluted to reach an absorbance of 0.5 in PBS, which corresponds to a cell density of approximately $1\times10^7$ CFU/mL. 100 µL of the diluted fungal inoculum was added to a 96-well plate. Serial two-fold dilutions of fluconazole in SDB were prepared, and 100 µL of each dilution (0.125-64 µM) was transferred to the wells, resulting in a final volume of 200 µL per well. A positive control comprising of the fungal inoculum and a negative control comprising of the SDB media were included. The plates were incubated at 37 °C for 72 h. The MIC was considered the lowest concentration of fluconazole that inhibited the visible growth of *C. albicans* and *C. krusei.* The experiments were performed in triplicate, and the results were analyzed statistically.

### *The minimum inhibitory and fungicidal concentrations of porphyrins*

The MIC of porphyrins was assessed using the broth microdilution method [41]. Working solutions of the PSs (**P-2H**, **P-Zn**, **P-InCl**, and **P-GaCl**) were prepared in concentrations of 5–40 µM in 5% DMSO in PBS. A 100 µL of the fungal suspensions with an OD of 0.5, corresponding to a cell density of approximately $1\times10^7$ CFU/m was added into the wells of a 96-well plate, and 100 µL of each PS solution was then added, resulting in a final volume of 200 µL per well. A positive control comprising of the fungal inoculum and a negative control comprising of the SDB media were included. The plates were placed on an LED device, irradiated for 60 min at a fluence rate of 0.05 W/cm$^2$ and irradiation dose of 180 J/cm$^2$, and incubated at 37 °C for 24 h. The MIC was determined as the lowest concentration of the PSs resulting in a significant inhibition of *C. albicans* and *C. krusei* growth compared to the positive control. The experiments were performed in triplicate, and the results were analyzed statistically. To determine the minimum fungicidal concentrations (MFC), 1µL aliquots from each well without visible fungal growth, along with positive and negative controls, were plated on SDA plates and incubated at 37 °C for 24 h. The MFC was defined as the lowest concentration that resulted in no fungal growth on the plate.

### *Photodynamic inactivation of Candida spp.*

*C. albicans* and *C. krusei* were inoculated in 5 ml SDB and grown aerobically at 37 °C for 24 h. Each culture was subsequently centrifuged at 45 g for 10 min, after which the pellet was washed twice with sterile distilled water and resuspended in PBS to achieve an OD of 0.5 (approximately $1\times10^7$ CFU/mL). A 100 µL of each *Candida spp.* was transferred into a 96-well plate. A 100 µL of each photosensitizer (**P-2H**, **P-Zn**, **P-InCl**, and **P-GaCl**) at MIC concentrations were added to each well. In addition, to determine whether the PS alone affected cell viability, additional wells containing yeast suspensions were sensitized with PSs under similar conditions but not irradiated. A positive control of the yeast suspensions neither sensitized with PSs nor exposed to LED light was included. The plate was incubated for 15 min in the dark, and then placed on an LED device and irradiated for 15, 30, 45, and 60 minutes at irradiation doses of 45, 90, 135, and 180 J/cm$^2$, respectively, and a fluence rate of 0.05 W/cm$^2$. The corresponding 96-well plates for dark toxicity studies were kept in the dark for 15 min. To determine cell survival, aliquots from each well were serially diluted 10-fold in PBS. 25 µl aliquots of these dilutions were spread on the surfaces of SDA plates. All plates were incubated aerobically at 37 °C for 24 h. Post-incubation, yeast colony counts were quantified and the results were expressed as colony-forming units per milliliter (CFU/ml). All the experiments were conducted in triplicate and the results were statistically analyzed.

### *Cell viability curve assay*

This was performed to determine the duration required for PSs to inhibit the growth of *C. albicans* and *C. krusei.* Based on the MIC of each of the porphyrins determined using the broth microdilution technique described in section 2.5.3, two 96-well plates were prepared with the following concentrations: ½MIC, MIC, and 2×MIC, as well as the positive (*C. albicans* and *C. krusei*) and negative (SDB) controls. One plate was exposed to light irradiation for 60 min at 37 °C, while the other plate was incubated in the dark at 37 °C. At various time points (0, 15, 30, 45, and 60 min), 10 µL aliquots were taken from the wells and seeded onto SDA plates, and the plates were incubated at 37 °C for 24 h. After incubation, the CFU was calculated and expressed in $Log_{10}$ CFU/mL. This assay provided insights into the time-dependent effects of the treatment on both *C. albicans* and *C. krusei* growth.

### *Combination therapy of PACT and fluconazole*

The combination therapy involved treating samples with the MIC dose of fluconazole, followed by porphyrin-Photodynamic Therapy (P-PDT) at a concentration equal to twice the MIC which represents a dose double the minimum concentration required to inhibit visible fungal growth (2xMIC), A 500 µL of *C. albicans* and *C. krusei* (approximately $1\times10^7$ CFU/mL) was added to 400 µL of SDB. Subsequently, fluconazole (4 µg/ml for *C. albicans*, 64 µg/ml for *C. krusei*), was added and the samples were incubated for 24 h at 37 °C. Following the incubation, the fluconazole-treated *C. albicans* and *C. krusei* were subjected to P-PDT as previously described. After P-PDT, the samples were diluted 1:5, and 50 µL aliquots from each sample were plated onto

SDA plates. The plates were incubated at 37 °C for 24 h. The percentage survival for each fluconazole-PDT treatment was determined by counting the CFU/mL. All the experiments were conducted in triplicate and the results were statistically analyzed.

### *Statistical analysis*

Statistical analysis was conducted using one-way analysis of variance (ANOVA) followed by Tukey's post-hoc test to compare group differences. Results were presented as mean ± standard deviation. Origin software (OriginPro 9.1, OriginLab Corporation) was used for the statistical analysis. A $p < 0.001$ was considered statistically significant.

## RESULTS AND DISCUSSION

### Synthesis and characterization of photosensitizers

**P-2H**, **P-Zn**, **P-InCl**, and **P-GaCl** were successfully synthesized as shown in Scheme 1, using the Adler-Longo method. Each of these compounds was characterized through spectroscopic methods, confirming successful synthesis and purity. The synthesis of **P-2H** yielded 13%, consistent with typical values (10–20%) reported in the literature for free base porphyrins [41, 42]. Zinc porphyrin (**P-Zn**) was synthesized with an 84% yield under mild conditions, demonstrating the efficiency of zinc incorporation. The synthesis of **P-InCl** utilized acetic acid as the reaction solvent. Acetic acid was chosen for its acidic properties, which facilitate the metallation process, and its high boiling point, supporting prolonged reflux conditions. This approach resulted in an 82% yield, consistent with reported yields (60–85%) for heavier metals in porphyrin complexes [44]. The synthesis process was validated by UV-Vis, MALDI- TOF-MS, $^1$H NMR, and FTIR analyses confirming the purity of each photosensitize (data is provided in Figs. S1–S12 in the supplementary data).

The observed mass spectrum for **P-2H** showed an m/z peak at 931.374 (Fig. S1). This corresponded well with the calculated mass for this compound of 930.34. The calculated elemental composition was as follows: C (56.81%), H (2.82%), and N (6.02%), and was close to the experimentally determined values: C (56.54%), H (2.64%), and N (6.10%). The $^1$H NMR spectrum of **P-2H** revealed significant deshielding at δ 8.87 ppm, corresponding to the β-pyrrole protons and suggesting strong anisotropic effects due to the porphyrin ring (Fig. S5). The aromatic protons were detected at δ 8.10 ppm with a coupling constant of 8.5 Hz, associated with the *ortho*-bromophenyl groups. The integration of this peak indicated the presence of eight protons, consistent with the substitution pattern of the bromophenyl groups. Another set of aromatic protons was observed at δ 7.90 ppm with a slightly higher coupling constant of 8.6 Hz, corresponding to the *meta*-bromophenyl protons. The deshielding at this position further supported the electronic influence of the bromine substituents. Lastly, the peak at δ -2.93 ppm was attributed to the inner NH protons, which are significantly shielded due to their position within the porphyrin ring, indicating the typical characteristics of a free-base porphyrin. The FTIR spectrum of **P-2H** featured a peak at 3307 $cm^{-1}$ corresponding to the N-H Stretching vibration of the inner pyrrole nitrogen atoms in the porphyrin ring, while the C-H stretching vibrations were observed at 2928 and 2867 (Fig. S9). The C-Br stretching vibrations within the porphyrin core are observed at 719 cm confirming the bromination of the porphyrin ring.

For **P-Zn**, the observed m/z peak was at 994.349, which aligned closely with the calculated mass of 994.69 (Fig. S2). The calculated elemental composition was as follows: C (53.18%), H (2.43%), and N (5.64%), and was close to the experimentally determined values: C (53.55%, H (2.75%), and N (5.52%). In the $^1$H NMR spectrum of **P-Zn**, the deshielding at δ 8.87 ppm corresponded to the β-pyrrole protons, indicating their proximity to the porphyrin ring's aromatic system (Fig. S6). The chemical shift of these protons was consistent with the typical effects observed in metallated porphyrins, where the metal center influences the electronic environment. The aromatic protons of the ortho-bromophenyl groups were seen at δ 8.10 ppm with a coupling constant of 8.5 Hz, which is consistent with the electron-withdrawing effects of the bromine atoms. The meta-bromophenyl protons appeared at δ 7.90 ppm, with a coupling constant of 8.6 Hz, showing similar deshielding effects as seen in the free-base porphyrin but with slight variations due to the presence of the zinc metal center. Notably, the absence of the peak at δ -2.93 ppm, which corresponded to the inner NH protons in the free-base porphyrin, confirmed the successful metallation of the porphyrin, as the metal center replaces the inner protons, leading to a disappearance of this signal in the spectrum. The FTIR spectra revealed peaks at 2919 $cm^{-1}$ and 2852 $cm^{-1}$ for C-H stretching vibrations, 989 $cm^{-1}$ for C-CH stretching, and 7161 $cm^{-1}$ for C-Br stretching (Fig. S10). The absence of the N-H stretch at 3300 $cm^{-1}$ further confirmed the metallation of the porphyrin core with Zinc.

The observed m/z peak for **P-InCl** was at 1078.30 $[M]^+$, which closely matched the calculated mass of 1078.59 (Fig. S3). Additionally, a peak at 1043.33 $[M\text{-}Cl]^+$ was detected, indicating the loss of the axial chloride ligand. Elemental analysis provided the following percentages: C (48.36), H (2.38), and N (5.47), which closely matched the theoretical values of C (49.00), H (2.24), and N (5.19). In the $^1$H NMR spectrum, significant deshielding was observed at δ 9.05 ppm, corresponding to the β-pyrrole protons (Fig. S7). The chemical shift at δ 9.05 ppm was slightly more downfield compared to the free-base and zinc-metallated porphyrins, suggesting a greater deshielding effect due to the indium atom. The aromatic protons of the ortho-bromophenyl groups

were detected at δ 8.18 ppm with a coupling constant of 8.4 Hz. Additionally, a broader range of signals between δ 7.98 ppm and δ 7.62 ppm corresponded to a mixture of meta- and ortho-bromophenyl protons. The multiplet nature of this signal suggested overlapping resonances of the protons in these positions, influenced by the electronic environment created by the indium center. This broadening is typical in metallated porphyrins, where the metal center induces changes in the electronic distribution across the porphyrin macrocycle causing splitting patterns in the aromatic region. The FTIR spectra of **P-InCl** indicated peaks at 2917 $cm^{-1}$ for C-H stretching vibrations, 997 $cm^{-1}$ for C-CH stretching, and 716 $cm^{-1}$ for C-Br stretching (Fig. S11). The absence of the N-H stretch at 3300 $cm^{-1}$ further confirmed the metallation of the porphyrin core with indium.

The observed m/z peak for **P-GaCl** was at 999.321, which aligned with the calculated mass of 1033.49, accounting for the possible loss of a chloride ion (Fig. S4). The experimental elemental analysis was as follows: C (51.64%), H (2.39%), and N (5.33%) which closely matched the calculated values C (51.14%), H (2.34%), and N (5.42%). In the $^{1}$H NMR spectrum, the most significant deshielding was observed at δ 9.11 ppm, corresponding to the β-pyrrole protons (Fig. S8). The aromatic protons of the bromophenyl groups were observed as a broad multiplet between δ 8.21 ppm and δ 7.82 ppm, corresponding to a total of 16 protons. This broad signal range indicated the overlapping of the ortho- and meta-bromophenyl protons. The FTIR spectra revealed peaks at 2921 $cm^{-1}$ (C-H stretching), 997 $cm^{-1}$ (C-CH bending), and 713 $cm^{-1}$ (C-Br stretching) (Fig. S12). The absence of an N-H stretch around 3300 $cm^{-1}$ confirmed the metallation of the porphyrin with gallium.

## Photophysical characterization of the photosensitizers

The Soret band (B band), is an absorption band in the UV-visible spectrum of porphyrins, typically appearing in the 400-450 nm range and is associated with the electronic transitions from the ground state to the second excited state (π-π* transition) [45]. On the other hand, Q bands are typically observed in the 500-700 nm range and are less intense compared to the Soret band. These bands arise from the π→π* transitions but involve higher energy orbitals [46]. The Soret bands for all four compounds were within the range of 418.5 nm to 430.5 nm. **P-2H** exhibited its Soret band at 418.5 nm, however, **P-Zn**, **P-InCl**, and **P-GaCl** displayed Soret bands (420, 430.5, and 420.5, respectively) that were slightly red-shifted (Fig. 1, Table 1). This shift can be attributed to the influence of the metal ion on the electronic structure of

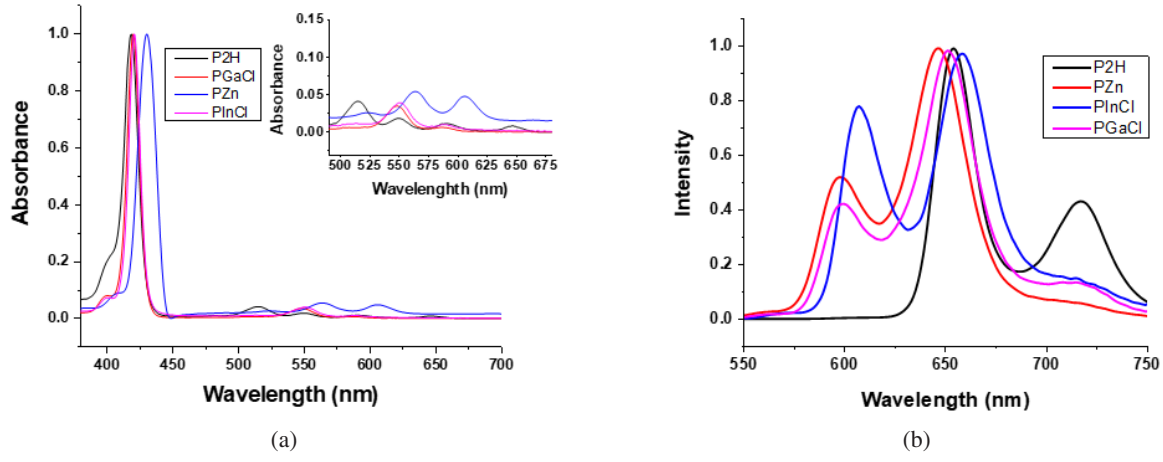


(a) (b)

**Fig. 1.** (a) Normalized UV absorption spectra of P-2H, P-Zn, P-InCl, and P-GaCl in DCM, at 25 °C, inset highlights the Q bands for each sample. (b) Normalized fluorescence emission spectra of P-2H, P-Zn, P-InCl, and P-GaCl, ($\lambda_{exc}$ = 418.5, 420, 430.5, and 420.5, respectively, and recorded from 500 to 750 nm in DMF).

**Table 1.** Photo-physical properties of **P-2H**, **P-Zn**, **P-InCl**, and **P-GaCl** photosensitizers.

| Compound | Soret band (nm) ($L\ mol^{-1}\ cm^{-1}$) | Q Bands (nm) ($L\ mol^{-1}\ cm^{-1}$) | | | | Emission ($\lambda_{max}$ nm) | $\Phi_F$ | ϕΔ |
|---|---|---|---|---|---|---|---|---|
| | | $Q_{y01}$ | $Q_{y00}$ | $Q_{x01}$ | $Q_{x00}$ | | | |
| **P-2H** | 418.5 ($4.88\times10^5$) | 515 ($2.29\times10^4$) | 549.5 ($1.82\times10^4$) | 590.5 ($1.50\times10^4$) | 646.5 ($1.34\times10^4$) | 654, 718 | 0.0016 | 0.11 |
| **P-Zn** | 420 ($4.84\times10^5$) | 548 ($2.54\times10^4$) | 587 ($1.18\times10^4$) | | | 598, 647 | 0.0005 | 0.28 |
| **P-InCl** | 430.5 ($1.93\times10^5$) | 561.5 ($1.13\times10^4$) | 609 ($0.414\times10^4$) | | | 607, 658 | 0.0002 | 0.52 |
| **P-GaCl** | 420.5 ($2.28\times10^5$) | 551 ($1.82\times10^4$) | 579 ($1.12\times10^4$) | | | 600, 651 | 0.0004 | 0.42 |

the porphyrin ring. The red-shift was more pronounced in **P-InCl**, where the Soret band is observed at 430.5 nm, indicating a significant impact of indium on the electronic delocalization within the porphyrin ring. For the Q bands, **P-2H** displayed four Q bands due to the splitting of the degenerate excited states, which is characteristic of free-base porphyrins [47]. Upon metalation, **P-Zn**, **P-InCl**, and **P-GaCl** the degeneracy was lifted, and the number of Q bands reduced to two, reflecting the D4h symmetry of the metallated porphyrins (Fig. 1a, inset). Therefore, metallation introduces significant changes in both the Soret and Q bands, primarily due to the effect of the metal ion on the conjugated π-electron system of the porphyrin ring [48]. Additionally, the type of metal, its ionic radius, and its electronic configuration play important roles in determining the shifts [49]. For example, **P-InCl** exhibited the most pronounced red-shift in both the Soret and Q bands, suggesting a greater interaction with the porphyrin ring, and this is consistent with similar studies, where heavier metals such as indium with larger ionic radii and lower electronegativity tend to cause more significant shifts in the absorption spectra of porphyrins [45, 46].

The fluorescence spectra of the four porphyrins (**P-2H**, **P-Zn**, **P-InCl**, and **P-GaCl**) exhibited characteristic emission peaks typical for porphyrins (see Fig. 1b). The emission maxima for each compound were red-shifted relative to their corresponding absorption maxima (Soret and Q bands). This red-shift, known as the Stokes shift, is common in porphyrins due to the relaxation of the excited state before photon emission [52]. For **P-2H**, the emission peaks at 654 nm and 718 nm corresponded to the transitions from the first excited state ($S_1$) to the ground state ($S_0$) (Table 1). These emission peaks suggest the presence of vibronic coupling, where emission occurs from different vibrational levels of the excited state [53]. However, metallation significantly affected the emission peaks. Where for **P-Zn**, **P-InCl**, and **P-GaCl**, the emission peaks shifted depending on the metal inserted. **P-Zn** exhibited emission peaks at 598 nm and 647 nm, **P-InCl** at 607 nm and 658 nm, and **P-GaCl** at 600 nm and 651 nm. These shifts are indicative of the influence of the metal on the electronic structure of the porphyrin ring, with **P-InCl** showing the most significant red shift among the metallated porphyrins. The emission spectrum of porphyrins often mirrors the absorption spectrum, due to the similarity in the vibrational structures of the ground and excited states [54]. The emission spectra of these porphyrins showed a mirror image relationship to their Q band absorptions, with slight variations, e, particularly in **P-InCl**. This is likely due to the more complex electronic interactions introduced by indium, which adds extra vibronic coupling [55]. The emission was broader and more red-shifted in **P-2H** compared to the metallated porphyrins, indicating that the free-base porphyrin has a more flexible electronic structure [56].

The bromine atoms at the *meso*-positions of the porphyrin ring in all four compounds introduced a heavy atom effect, which promoted ISC and reduced $\Phi_F$ [57]. **P-2H** exhibited a relatively low $\Phi_F$ of 0.0016 (Table 1), which can be attributed to the heavy atom effect of the bromine substituents, which facilitate ISC from the singlet excited state to the triplet state, thus reducing the efficiency of fluorescence. However, for the metallated porphyrins (**P-Zn**, **P-InCl**, and **P-GaCl**), the effect of bromine was compounded by the influence of the metal ion at the core. The heavy atom effect of bromine, combined with the metal's electronic properties, further enhanced non-radiative processes, leading to even lower $\Phi_F$ [58]. The $\Phi_F$ for **P-Zn** was 0.0005, significantly lower than that of **P-GaCl**, and **P-InCl** had the least at 0.0002 (Table 1). This very low quantum yield in **P-InCl** was due to a balance between the heavy atom effect of indium and the electronic structure stabilization it provides, which favors non-radiative decay pathways leading to a significant reduction in fluorescence efficiency. The $\Phi_F$ for **P-GaCl** was 0.0004, indicating gallium's electronic influence, combined with the heavy atom effect of bromine, strongly favoring non-radiative decay processes.

Singlet oxygen quantum yield is a measure of the efficiency with which a photosensitizer, upon light absorption, can transfer energy from its excited triplet state to molecular oxygen, resulting in the formation of singlet oxygen ($^1O_2$) [56, 57]. Singlet oxygen is a highly reactive oxygen species that plays an important role in PACT. In this study, **P-2H** exhibited the lowest φΔ of 0.11 among the four compounds (Table 1). While the presence of bromine atoms enhanced ISC through the heavy atom effect, the absence of a metal ion resulted in the lack of additional stabilization of the triplet state to facilitate more efficient singlet oxygen production. For **P-Zn**, the d10 electronic configuration of zinc led to the stabilization of the excited states, particularly the triplet state, leading to a moderate increase in φΔ compared to **P-2H**. **P-InCl** exhibited the highest φΔ, because indium being a heavy metal, significantly enhanced ISC due to the strong heavy atom effect. This effect facilitates the transition from the singlet state to the triplet state, which is important for efficient singlet oxygen generation [61]. Similar to **P-InCl**, gallium in **P-GaCl** also exhibited a strong heavy atom effect, enhancing ISC and stabilizing the triplet state. An inverse relationship between $\Phi_F$ and φΔ was reported, where a higher $\Phi_F$ indicates that a larger proportion of the excited state energy is released as fluorescence, leaving less energy available for ISC and, consequently, for singlet oxygen production [62]. Conversely, a lower $\Phi_F$ suggests that more energy is diverted to the triplet state via ISC, increasing the potential for singlet oxygen generation. Therefore, the φΔ in the four compounds was significantly influenced by both the heavy atom effect of bromine substituents and the nature of the metal ion inserted into the porphyrin core.

## Photodynamic antimicrobial and combined therapies

### *MIC and MFC analysis*

The MIC and MFC values obtained for the photosensitizers in this study indicate that **P-InCl** exhibited the most potent antifungal activity against *C. albicans*, with both MIC and MFC values as low as 5 µM (Table 2). This suggests that **P-InCl** is highly effective in inhibiting the growth of this strain and causing cell death at low concentrations when irradiated. The strong antifungal activity observed for **P-InCl** can be attributed to its efficient photodynamic action, involving the generation of reactive oxygen species (ROS) that cause oxidative damage to the cell walls and internal structures of fungal cells, leading to cell death [63]. **P-GaCl** also showed significant activity with MIC and MFC values of 15 µM, indicating its potential as a photosensitizer, though slightly less effective than **P-InCl** (Table 2). **P-Zn** demonstrated moderate antifungal activity with MIC values of 20 µM against *C. albicans*. The higher MIC and MFC values compared to **P-InCl** and **P-GaCl** were related to the zinc metallation, which impacted the solubility and cellular uptake of the porphyrin, thus requiring higher concentrations to achieve effective photodynamic inactivation. **P-2H** showed the least antifungal activity against *C. albicans*, with an MIC and MFC of 30 µM. The absence of metal in **P-2H** resulted in lower ROS generation under irradiation, requiring higher doses to reach effective photoinactivation levels. All the photosensitizers generally showed less effectiveness against *C. krusei*, with **P-InCl** again showing the lowest MIC and MFC values (15 µM). However, both **P-2H** and **P-Zn** had MIC values exceeding 40 µM, indicating a significantly reduced antifungal effect. The difference in efficacy between the photosensitizers against the two Candida species could be due to variations in cell structures and metabolic activities which affect the uptake and interaction of the photosensitizers [57, 58].

The MIC of fluconazole indicated significant differences in its effectiveness against C. *albicans* and C. *krusei*. For *C. albicans*, the MIC was 4 µM, reflecting fluconazole's effectiveness with a relatively low concentration needed to inhibit growth (Table 2). The MFC for *C. albicans* was 8 µM, suggesting that while 4 µM was sufficient to inhibit growth, a higher concentration of 8 µM was required to achieve complete fungal cell death. However, *C. krusei* exhibited high resistance to fluconazole, with both MIC and MFC values exceeding 64 µM, highlighting fluconazole's limited efficacy against this strain. Although the MIC of fluconazole for *C. albicans* is relatively low at 4 µM, meaning it can inhibit growth at slightly lower concentrations than P-InCl, achieving complete eradication with fluconazole typically requires prolonged exposure, often spanning several days. This extended treatment period is necessary because fluconazole works by inhibiting fungal cell growth rather than killing the cells outright, making fungal eradication a slower process. In contrast, P-InCl under PACT provides rapid action, with complete fungal eradication observed within just 30 minutes of irradiation, due to the immediate production of reactive oxygen species (ROS) upon light activation, which directly damages fungal cell structures and leads to rapid cell death. Therefore, while fluconazole alone may be effective over a long treatment period, the combined therapy offers a faster, more efficient solution that minimizes the time required for fungal elimination, reduces the risk of recurrence, and potentially lowers overall drug exposure.

**Table 2.** MIC and MFC values (µM) of P-2H, P-Zn, P-InCl, and P-GaCl against *C. albicans* and *C. krusei*.

| Compound | *C. albicans* | | *C. krusei* | |
|---|---|---|---|---|
| | MIC (µ*M*) | MFC (µ*M*) | MIC (µ*M*) | MFC (µ*M*) |
| **P-2H** | 30 | 30 | > 40 | > 40 |
| **P-Zn** | 20 | 25 | 35 | > 40 |
| **P-InCl** | 5 | 5 | 15 | 15 |
| **P-GaCl** | 15 | 15 | 20 | 25 |
| **Fluconazole** | 4 | 8 | > 64 | > 64 |

### *Photodynamic inactivation of C. albicans and C. krusei*

The photodynamic inactivation (PDI) of *C. albicans* and *C. krusei* was investigated using four different porphyrins (**P-2H**, **P-Zn**, **P-InCl**, and **P-GaCl**) at their MIC values under varying irradiation times (0, 15, 30, 45, and 60 minutes) (Fig. 2). The survival curves demonstrated that no significant toxicity was observed for the cells treated with these porphyrins for 60 minutes in the dark,

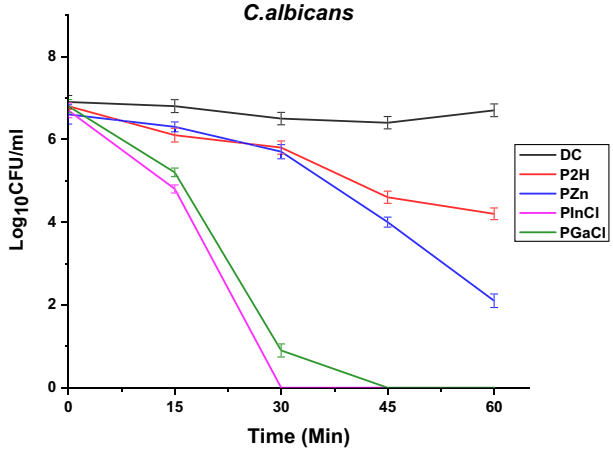


**Fig. 2.** Photodynamic inactivation of *C. albicans* under light irradiation (0.05 W/cm$^2$ and total light dosage of 180 J/cm$^2$ for 60 min), DC: Dark control. Data are mean values and standard error from three replicate experiments; analyzed by two-way ANOVA ($p < 0.05$).

as expected. Additionally, irradiation in the absence of porphyrins did not affect cell viability, confirming that the photoinactivation was solely dependent on the presence and concentration of the porphyrins. For **P-InCl** at its MIC, a rapid and significant reduction in cell viability was observed, achieving nearly a 5-log reduction after 30 minutes of irradiation (Fig. 2). **P-GaCl** also demonstrated strong activity, achieving a 4-log reduction within 30 minutes, with no viable cells detected after 45 minutes. **P-Zn** and **P-2H** demonstrated lower photodynamic activity against *C. albicans*, with **P-Zn** achieving a maximum 3-log reduction and **P-2H** showing about a 2-log reduction after 60 minutes of irradiation.

For *C. krusei*, the PDI experiments were conducted under similar conditions, with MIC values slightly higher than those observed for *C. albicans*, reflecting the inherent resistance of *C. krusei*. The survival curves indicate a significant photodynamic effect dependent on both the irradiation time and the specific porphyrin used. Initial observations revealed no significant toxicity in the dark, suggesting that the porphyrins alone did not affect the viability of *C. krusei* cells without light activation. Upon light exposure, a time-dependent decrease in *C. krusei* viability was observed, with **P-InCl** demonstrating the most significant reduction (Fig. 3). After 15 minutes of irradiation, **P-InCl** caused a decrease of approximately 1.9 log in cell viability. This effect intensified with longer irradiation times, where 30 minutes resulted in a 2.8-log reduction, and 45 minutes caused a dramatic 4.5-log reduction, indicating a near-complete eradication of the cells. By 60 minutes, both **P-InCl** and **P-GaCl** achieved complete inactivation, demonstrating their high photodynamic efficacy. In contrast, **P-2H** and **P-Zn** exhibited lower effects, with log reductions of around 1.7 and 2.1, respectively, after 60 minutes of irradiation. These results suggest that metallation of the porphyrin core significantly enhanced the photodynamic properties, with indium and gallium derivatives being particularly more effective. The differences in the log reductions across the different porphyrins for both *C. albicans* and *C. krusei* were statistically significant ($p<0.05$).

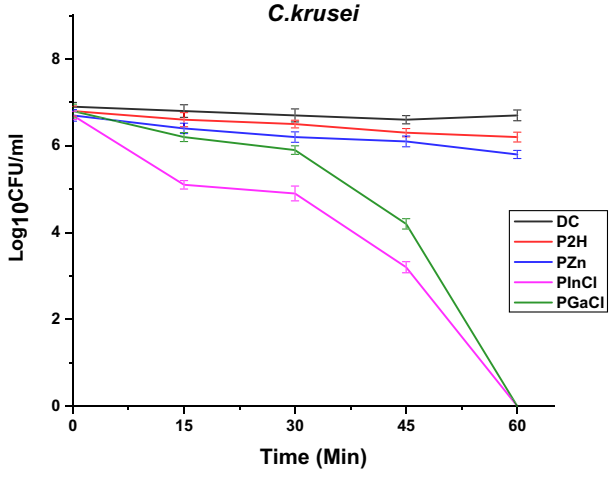


**Fig. 3.** Photodynamic inactivation of *C. krusei* under light irradiation (0.05 W/cm$^2$ and total light dosage of 180 J/cm$^2$ for 60 min). Data are mean values and standard error from three replicate experiments; analysed by two-way ANOVA ($p<0.05$).

**P-2H** and **P-Zn** demonstrated lower efficiency in terms of photoinactivation, exhibiting minimal cytotoxic effects on fungal cells (Figs. 2 and 3), the MIC and MFC were also not favorable as the required dosage for effective photo-inactivation were relatively high (Table 2). Therefore, subsequent studies were performed on **P-InCl** and **P-GaCl**.

### *Cell viability curve test*

The cell viability assay was performed to assess the photodynamic inactivation efficacy of the two metallated porphyrins, **P-InCl** and **P-GaCl** against *C. albicans* and *C. krusei* at MIC concentrations (1/2 MIC, MIC, and 2xMIC). The assay results were expressed by the viable cell count on a logarithmic scale, compared to the positive growth control (Fig. 4), to determine the time-dependent fungicidal activity, and data were presented as mean values and standard error from three replicate experiments; analyzed by two-way ANOVA ($p<0.05$). When *C. albicans* was treated with **P-InCl** and **P-GaCl** at the previously defined MIC concentrations (1/2 MIC, MIC, and 2xMIC) under light irradiation, significant photoinactivation was observed. At the highest concentration of 2xMIC, complete eradication of viable cells was noted within the first 15 minutes of exposure for **P-InCl**, and 45 minutes for **P-GaCl**. This rapid decline in CFU/mL in **P-InCl** indicated that it was highly effective at generating reactive oxygen species (ROS) upon light activation, leading to the destruction of fungal cells. However, at concentrations equivalent to 1/2MIC and MIC, while there was some reduction in CFU/mL, complete photoinactivation was not achieved within the same timeframe, indicating a dose-dependent response.

Under white-light conditions, both **P-InCl** and **P-GaCl** demonstrated significant photodynamic activity against *C. krusei*. However, similar to what was observed with *C. albicans*, **P-InCl** exhibited superior efficacy compared to **P-GaCl**. At the highest tested concentration (2xMIC), **P-InCl** achieved a more rapid and complete reduction in CFU/mL within 30 minutes of light exposure. In comparison, **P-GaCl** also displayed photodynamic inactivation but required a longer time of 45 minutes to achieve similar levels of fungicidal activity. In dark conditions, neither **P-InCl** nor **P-GaCl** showed significant antifungal activity, an indication that the photodynamic mechanism relies on light activation to generate ROS. Therefore, in both *C. albicans* and *C. krusei*, **P-InCl** performed better than **P-GaCl** in terms of photodynamic inactivation. While both fungi showed susceptibility to photodynamic inactivation, the degree of susceptibility differed slightly. *C. krusei* appeared to be more resistant than *C. albicans*

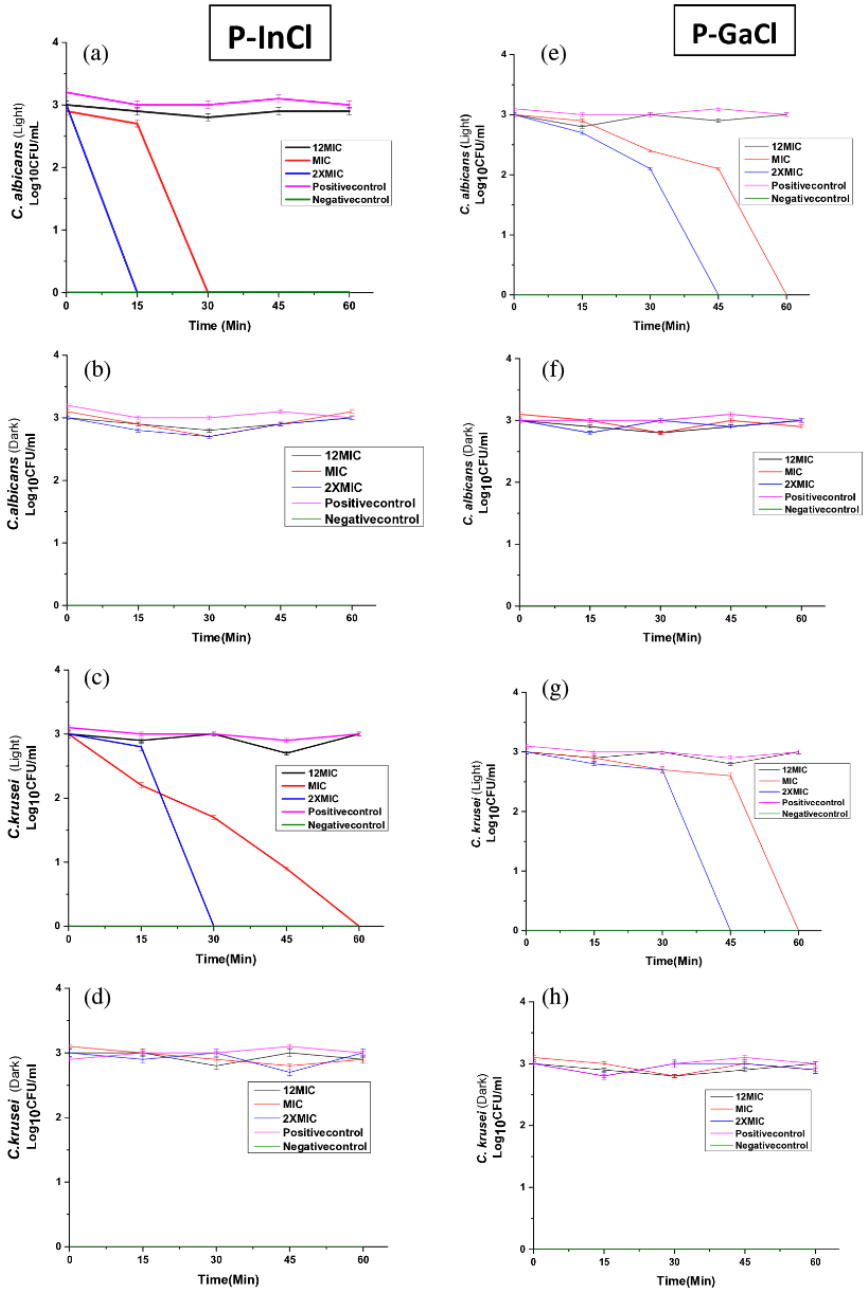


**Fig. 4.** Cell viability curve of **P-InCl** and **P-GaCl** against *C. albicans* and *C. krusei* under white-light irradiation (0.05 W/cm$^2$ and total light dosage of 180 J/cm$^2$) and in dark conditions for 60 Min.

under similar conditions, requiring higher concentrations or longer exposure times for complete eradication.

The lack of significant reduction in CFU/mL at MIC and 1/2MIC concentrations under dark conditions suggests that the intrinsic antifungal properties of these metalloporphyrins are minimal and that their efficacy is predominantly driven by light-induced photodynamic action. Both indium and gallium are group 13 elements and share similar properties, but they differ in their electronic configurations [66]. Indium has a larger atomic radius and a different d-orbital configuration compared to gallium, and this difference influences how these metals interact with the porphyrin ligand, affecting the overall electronic structure of the metalloporphyrin complex [50]. Indium, with its larger ionic radius, can cause a more significant distortion of the porphyrin ring, potentially leading to a greater degree of conjugation and more efficient absorption of light [67]. This enhanced light absorption can increase the production of singlet oxygen ($^1O_2$) and other reactive oxygen species (ROS), which are crucial for the photodynamic inactivation of microorganisms.

### *Combined treatment of fluconazole and PACT on Candida spp*

The study examined the effects of combination therapy with fluconazole followed by porphyrin-Photodynamic Therapy (P-PDT) on *C. albicans* and *C. krusei*. The results revealed a time-dependent decrease in cell viability when using **P-InCl** and **P-GaCl** porphyrins (2xMIC) in P-PDT, with *C. albicans* showing more significant log reductions compared to *C. krusei*. Fluconazole treatment resulted in moderate reductions in *C. albicans* viability but had a minimal effect on *C. krusei*, highlighting its notable resistance to fluconazole. However, when fluconazole was combined with **P-InCl** or **P-GaCl** in P-PDT, a synergistic effect was observed, leading to significant log reductions in both fungal species ($p<0.05$). The combination therapy significantly enhanced antifungal activity compared to individual treatments, particularly at longer irradiation times, where the reduction in CFU/ml was more pronounced ($p<0.05$).

For *C. albicans*, fluconazole alone showed limited effectiveness, with only a slight reduction in CFU/mL across all time points (Fig. 5). However, **P-InCl** alone demonstrated significant photodynamic activity, as cell viability dropped to zero after just 15 minutes of irradiation, suggesting a potent effect, likely due to its high singlet oxygen generation efficiency and strong interaction with fungal cells. **P-GaCl** also showed significant activity, though slightly less than **P-InCl**, with complete reduction achieved after 30 minutes ($p<0.05$), possibly due to differences in photophysical properties or cellular uptake efficiency. The combined treatments (**P-InCl**+Fluconazole and **P-GaCl**+Fluconazole) achieved a 6-log reduction by 15 minutes, indicating complete eradication of the fungal population. This synergistic effect can be attributed to the dual mechanisms, where fluconazole disrupts ergosterol biosynthesis in the

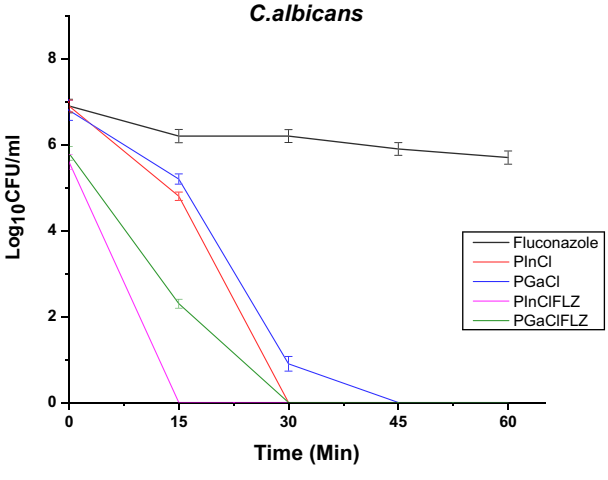


**Fig. 5.** Fungicidal activity of combined treatment of fluconazole and PACT on *C. albicans*. Data are mean values and standard error from three replicate experiments; analysed by two-way ANOVA ($p<0.05$).

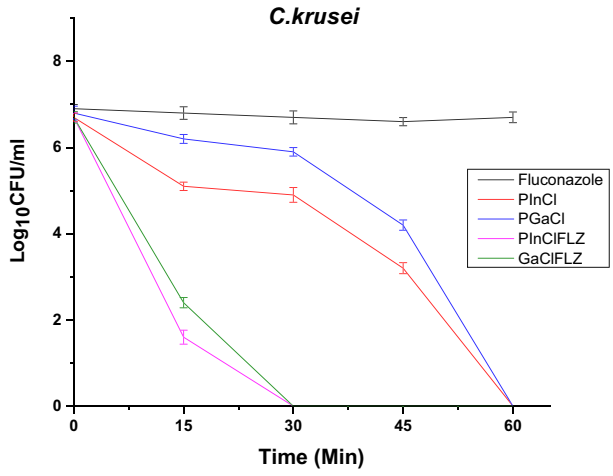


**Fig. 6.** Fungicidal activity of combined treatment of fluconazole and PACT on *C. krusei*. Data are mean values and standard error from three replicate experiments; analysed by two-way ANOVA ($p<0.05$).

fungal membrane, enhancing membrane permeability, which facilitates greater uptake of the porphyrin compounds. Upon irradiation, the PSs generated ROS that damaged cellular components, including lipids, proteins, and nucleic acids, leading to rapid cell death. The combination likely enhanced oxidative damage while simultaneously targeting fungal growth pathways, resulting in accelerated eradication.

For *C. krusei*, known for its resistance to fluconazole, the monotherapy with fluconazole was largely ineffective, showing minimal reduction in CFU/mL, consistent with the MIC data (Fig. 6). Additionally, **P-InCl** alone provided a moderate reduction in viability, with significant effects observed by 45 minutes of irradiation ($p<0.05$). **P-GaCl** was slightly less effective than **P-InCl** but still managed to achieve a complete reduction after 45 minutes. However, for combined treatments, the log reductions were slightly less, with approximately 4 to 5 log reductions at 15 minutes and complete eradication by 30 minutes for both **P-InCl** and **P-GaCl**. This demonstrates that while *C. krusei* is more resistant, the combination therapy still effectively eradicates the fungal cells within 30 minutes of light exposure.

## CONCLUSION

This study demonstrates the antifungal efficacy of porphyrin-based PACT, particularly when combined with fluconazole, against *C. albicans* and *C. krusei.* The heavy atom effect, coupled with the metallation of the porphyrin core, played a significant role in enhancing the generation of ROS, which is essential for effective photodynamic inactivation. This was supported by the high efficacy of indium and gallium-metallated porphyrins (**P-InCl** and **P-GaCl**, respectively) in photodynamic inactivation, with **P-InCl** exhibiting the most pronounced antifungal

activity. The MIC and MFC analyses reveal that **P-InCl** was highly effective against *C. albicans* and *C. krusei*, achieving significant reductions in cell viability at low concentrations and short irradiation times. The combination of fluconazole with **P-InCl** or **P-GaCl** enhanced the overall antifungal efficacy, achieving complete eradication of *C. albicans* within 15 minutes of irradiation and overcoming the inherent resistance of *C. krusei* to fluconazole monotherapy. These findings highlight the potential of combining PACT with conventional antifungal agents like fluconazole to enhance treatment outcomes, particularly in cases involving drug-resistant fungal strains. The synergistic effect observed in this study suggests that such combination therapies could reduce the required dosages of antifungal drugs, minimize treatment durations, and address the growing concern of antifungal resistance.

### Author contributions

The conceptualization of this study was done by E.A.The methodological approach included syntheses and characterization of the porphyrins conducted by M.M, E.A and Biological studies were performed by M.M, B.M, and E.M. The manuscript was prepared by M.M, E.A, B.M, and E.M. Project administration and funding acquisition were done by E.A. All authors have reviewed and consented to the final version of the manuscript for publication.

### Funding

This work was financially supported by the South Africa/Canada/Kenya research chair's trilateral partnerships initiative, through funding from the International Development Research Foundation (IDRC), Canada (UID 108569-001).

### Acknowledgments

Sincere gratitude to Prof. Tebello Nyokong at Rhodes University for her invaluable support in mass spectrometry, NMR, and elemental analysis. Special thanks to USIU-Africa for generously providing laboratory space, instrumentation, and resources crucial to the success of this research.

### Conflicts of interest

The authors declare no conflict of interest.

### Supporting information

Details for the characterization of the porphyrins, along with their corresponding mass spectra, $^{1}$H NMR, and FTIR spectra are available as supporting information (Figs. S1–S12).This material is available free of charge via the Internet at http://www.worldscientific.com/doi/suppl/10.1142/S1088424625500130

## REFERENCES

1. Macias-Paz IU, Pérez-Hernández S, Tavera-Tapia A, Luna-Arias JP, Guerra-Cárdenas JE and Reyna-Beltrán E. *Rev. Argent. Microbiol.* 2023; **55**: 189–198.
2. Lopes JP and Lionakis MS. *Virulence* 2022; **13**: 89–121.
3. Li H, Miao M, Jia C, Cao Y, Yan T, Jiang Y and Yang F. *Front. Microbiol.* 2022; **13**: 930495.
4. Seyoum E, Bitew A and Mihret A. *BMC Infect. Dis.* 2020; **20**: 1–9.
5. Gómez-Gaviria M and Mora-Montes HM. *Infect. Drug Resist.* 2020: 1673–1689.
6. Jamiu AT, Albertyn J, Sebolai OM and Pohl CH. *Med. Mycol.* 2021; **59**: 14–30.
7. Nguyen TA, Kim HY, Stocker S, Kidd S, Alastruey-Izquierdo A, Dao A, Harrison T, Wahyuningsih R, Rickerts V and Perfect J. *Med. Mycol.* 2024; **62**: myad132.
8. Sardi JCO, Scorzoni L, Bernardi T, Fusco-Almeida AM and Mendes Giannini MJS. *J. Med. Microbiol.* 2013; **62**: 10–24.
9. Roudbary M, Vahedi-Shahandashti R, Santos ALS dos, Roudbar Mohammadi S, Aslani P, Lass-Flörl C and Rodrigues CF. *Crit. Rev. Microbiol.* 2022; **48**: 197–221.
10. Kaur J and Nobile CJ. *Curr. Opin. Microbiol.* 2023; **71**: 102237.
11. Reddy GKK, Padmavathi AR and Nancharaiah Y V. *Curr. Res. Microb. Sci.* 2022; **3**: 100137.
12. Mattingly AN, Gianturco SL, Pavlech LL, Storm KD and Yuen M V. 2021.
13. Perfect JR and Ghannoum M. *Infect. Dis. Clin.* 2020; **34**: 921–943.
14. Nivoix Y, Ledoux M-P and Herbrecht R. In Seminars in Respiratory and Critical Care Medicine. Vol 41. Thieme Medical Publishers, 2020; 158–174.
15. Denning DW. *Eur. J. Hosp. Pharm.* 2022; **29**: 109–112.
16. Garvey M and Rowan NJ. *Int. J. Mol. Sci.* 2023; **24**: 1584.
17. Eichner A, Gonzales FP and Maisch T. *Handb. Photomed.* 2013: 385.
18. Ilizirov Y, Formanovsky A, Mikhura I, Paitan Y, Nakonechny F and Nisnevitch M. *Molecules* 2018; **23**: 3152.
19. Sabino CP, Ribeiro MS, Wainwright M, Dos Anjos C, Sellera FP, Dropa M, Nunes NB, Brancini GTP, Braga GUL and Arana-Chavez VE. *Photochem. Photobiol.* 2023; **99**: 742–750.
20. Brancini GTP, Rodrigues GB, Rambaldi M de SL, Izumi C, Yatsuda AP, Wainwright M, Rosa JC and Braga GÚL. *Photochem. Photobiol. Sci.* 2016; **15**: 1503–1513.
21. Liu C, Hu M, Zeng X, Nair SP and Xu J. *Future Microbiol.* 2016; **11**: 351–362.
22. Fan F, Liu Y, Liu Y, Lv R, Sun W, Ding W, Cai Y, Li W, Liu X and Qu W. *Int. J. Antimicrob. Agents* 2022; **60**: 106673.

 

23. Rocca DM, Vanegas JP, Fournier K, Becerra MC, Scaiano JC and Lanterna AE. *RSC Adv.* 2018; **8**: 40454–40463.
24. Shetty H, Shukla V, Lokur AS and Chaughule RS. In Applications of Nanotechnology in Microbiology. Springer, 2024; 229–270.
25. Malatesti N, Munitic I and Jurak I. *Biophys. Rev.* 2017; **9**: 149–168.
26. Murage MW, Amuhaya EK, Mbatia BN, Muge EK and Derese S. *J. Porphyrins Phthalocyanines* 2024; **28**: 391–417.
27. Alves E, Faustino MAF, Neves MG, Cunha A, Nadais H and Almeida A. *J. Photochem. Photobiol. C Photochem. Rev.* 2015; **22**: 34–57.
28. Imran M, Ramzan M, Qureshi AK, Azhar Khan M and Tariq M. *Biosensors* 2018; **8**: 1–17.
29. Cormick MP, Alvarez MG, Rovera M and Durantini EN. *Eur. J. Med. Chem.* 2009; **44**: 1592–1599.
30. Quiroga ED, Mora SJ, Alvarez MG and Durantini EN. *Photodiagnosis Photodyn. Ther.* 2016; **13**: 334–340.
31. Soman R, Raghav D, Sujatha S, Rathinasamy K and Arunkumar C. *Rsc Adv.* 2015; **5**: 61103–61117.
32. Ravikumar M, Kathiravan A, Neels A and Mothi EM. *Eur. J. Inorg. Chem.* 2018; **2018**: 3868–3877.
33. Chumakov DE, Khoroshutin AV, Anisimov AV and Kobrakov KI. *Chem. Heterocycl. Compd.* 2009; **45**: 259–283.
34. Pham TC, Nguyen VN, Choi Y, Lee S and Yoon J. *Chem. Rev.* 2021; **121**: 13454–13619.
35. Oyim J, Omolo CA and Amuhaya EK. *Front. Chem.* 2021; **9**.
36. Bhatti M, Bhatti W and Mast E. *Inorg. Nucl. Chem. Lett.* 1972; **8**: 133–137.
37. Fery-Forgues S and Lavabre D. *J. Chem. Educ.* 1999; **76**: 1260.
38. Karolczak J, Kowalska D, Lukaszewicz A, Maciejewski A and Steer RP. *J. Phys. Chem. A* 2004; **108**: 4570–4575.
39. Makola LC, Managa M and Nyokong T. *Photodiagnosis Photodyn. Ther.* 2020; **30**: 101736.
40. Arastehfar A, Daneshnia F, Salehi M, Yaşar M, Hoşbul T, Ilkit M, Pan W, Hagen F, Arslan N and Türk-Dağı H. *Mycoses* 2020; **63**: 911–920.
41. Hlapisi N, Maliehe TS, Oluwafemi OS, Songca SP, Linganiso L and Motaung TE. *Pharmacogn. J.* 2021; **13**.
42. Ivanova YB, Chizhova NV, Khrushkova YV, Rusanov AI and Mamardashvili NZ. *Russ. J. Gen. Chem.* 2019; **89**: 459–465.
43. Alonso-Castro AJ, Zapata-Morales JR, Hernández-Munive A, Campos-Xolalpa N, Pérez-Gutiérrez S and Pérez-González C. *Bioorg. Med. Chem.* 2015; **23**: 2529–2537.
44. Nasri H. In 2020 IEEE International Conference on Design & Test of Integrated Micro & Nano-Systems (DTS). IEEE, 2020; 1–6.
45. Giovannetti R. *Macro to nano Spectrosc.* 2012: 87–108.
46. Zhao L, Wagner P, van der Salm H, Clarke TM, Gordon KC, Mori S and Mozer AJ. *J. Phys. Chem. C* 2015; **119**: 5350–5363.
47. Rukin P, Prezzi D and Rozzi CA. *J. Chem. Phys.* 2023; **159**.
48. Isaiah BM, Amuhaya EK and Muhanji CI. *J. Porphyrins Phthalocyanines* 2023; **27**: 819–837.
49. Yu W and Zheng S. *Spectrochim. Acta Part A Mol. Biomol. Spectrosc.* 2022; **282**: 121676.
50. Brothers PJ and Ghosh A. *Fundam. Porphyr. Chem. A 21st Century Approach* 2022; **1**: 141–240.
51. Gorduk S. *J. Porphyrins Phthalocyanines* 2020; **24**: 548–562.
52. Sajjadinezhad SM, Boivin L, Bouarab K and Harvey PD. *Coord. Chem. Rev.* 2024; **510**: 215794.
53. Chang M-H, Hoffmann M, Anderson HL and Herz LM. *J. Am. Chem. Soc.* 2008; **130**: 10171–10178.
54. Mojarrad AG and Zakavi S. *New J. Chem.* 2020; **44**: 3028–3037.
55. Lopes JMS, Sampaio RN, Ito AS, Batista AA, Machado AE da H, Araujo PT and Neto NMB. *Spectrochim. Acta Part A Mol. Biomol. Spectrosc.* 2019; **215**: 327–333.
56. Li X-Y, Zhang C-R, Wu Y-Z, Zhang H-M, Wang W, Yuan L-H, Yang H, Liu Z-J and Chen H-S. *Int. J. Mol. Sci.* 2015; **16**: 27707–27720.
57. Walker FA and Simonis U. *Encycl. Inorg. Chem.* 2006; **4**: 2390–2521.
58. Zhang X, Chen X, Sun Y and Zhao J. *Org. Biomol. Chem.* 2024.
59. Wang X, Lv H, Sun Y, Zu G, Zhang X, Song Y, Zhao F and Wang J. *Spectrochim. Acta Part A Mol. Biomol. Spectrosc.* 2022; **279**: 121447.
60. Nifiatis F, C Athas J, Don Dasitha Gunaratne K, Gurung Y, Mae Monette K and Joseph Shivokevich P. *Open Spectrosc. J.* 2011; **5**.
61. Topkaya D, Arnoux P and Dumoulin F. *J. Porphyrins Phthalocyanines* 2015; **19**: 1081–1087.
62. Li Z, Wang D, Xu M, Wang J, Hu X, Anwar S, Tedesco AC, Morais PC and Bi H. *J. Mater. Chem. B* 2020; **8**: 2598–2606.
63. Almeida LM, Zanoelo FF, Castro KP, Borissevitch IE, Soares CMA and Gonçalves PJ. *Photochem. Photobiol.* 2012; **88**: 992–1000.
64. Queiroga AS, Trajano VN, Lima EO, Ferreira AFM and Limeira Jr FA. *Photodiagnosis Photodyn. Ther.* 2011; **8**: 332–336.
65. Craig R a, McCoy CP, Gorman SP and Jones DS. *Expert Opin. Drug Deliv.* 2015; **12**: 85–101.
66. Aldridge S and Downs AJ. The Group 13 Metals Aluminium, Gallium, Indium, and Thallium: Chemical Patterns and Peculiarities. John Wiley & Sons; 2011.
67. Dechan P, Bajju GD, Sood P and Dar UA. *J. Mol. Struct.* 2019; **1183**: 87–99.